Nanoscience and Nanotechnology 2024, 13(2): 17-27
DOI: 10.5923/j.nn.20241302.01

A DFT Investigation of RE (Ce, Dy, Eu) Doped Monolayer ZnO for Potential Application in Dye Sensitized Solar Cells Application

Irungu M. Kahura[1,*], Kiprotich Sharon[1], Winfred M. Mulwa[2]

[1]Department of Physical and Biological Sciences, Murang'a University of Technology, Murang'a, Kenya
[2]Department of Physics, Egerton University, Egerton, Kenya

Abstract Utilizing density functional theory (DFT), a comparative study has been performed on monolayer ZnO (M-ZnO) doped with rare earth elements (RE=Ce, Dy and Eu) for potential application as a photoanode of a dye sensitized solar cell (DSSC). The implementation of the Quantum Espresso code facilitated the optimization of the structural configuration, allowing for the computation of a diverse array of properties, including the structural, electronic, optical, and electrical conductivity. Analysis on the formation energies indicated that RE (Ce, Dy and Eu) doped M-ZnO maintains a stable energetic configuration with Dy doping yielding the most stable compound of M-ZnO. In GGA +U formalism, an investigation into the electronic structure revealed a direct band gap energy values of 3.38, 3.19, 3.14 and 3.24 eV for undoped, Ce, Dy and Eu doped M-ZnO respectively. The Fermi level transitioned to the conduction band, signifying n-type properties. Furthermore, these compounds exhibited exceptional optical characteristics, notably a significant absorption coefficient that varied between 10^5 cm^{-1} and 10^6 cm^{-1}. The BoltzTrap code was employed to calculate electrical conductivity. Results demonstrate that the conductivity is significantly enhanced following the doping process. Accordingly, it is justifiable to state that RE (Ce, Dy and Eu) doped M-ZnO possess significant potential for application in DSSC technology.

Keywords Monolayer ZnO, Rare Earth elements, DFT, DSSC, Quantum Espresso

1. Introduction

ZnO has become a focal point of research and is extensively being utilized in the fabrication of solar cells [1], light emitting diodes [2], photocatalysis [3,4] photodetectors [5] and photovoltaics [6,7]. ZnO is presently regarded as the most viable semiconductive alternative to TiO_2 for use in the DSSC's photoanodes. Exhibiting a wide band gap of 3.37 eV, non-toxic properties, and a strong exciton energy of 60 meV, ZnO demonstrates exceptional features desirable in DSSC. Moreover, it is marked by high transparency in the visible spectrum, strong piezoelectric and photoelectric properties, outstanding electrical conductivity, and remarkable chemical and mechanical stability [8,9]. Recently, there has been significant research focused on low-dimensional ZnO-based nanostructures, including nanosheets, nanoparticles, nanorods, nanowires, and nanoribbons, owing to their promising applications in DSSCs [10-13]. Particularly, 2D ZnO nanostructures have demonstrated unique properties that deviate from that of their bulk phases counterparts. Their desirable chemical and physical properties generate a combination of enhanced photoelectron mobility, increased surface area for dye adsorption resulting into improved power conversion efficiency (PCE) [14].

Consequently, the fascination with 2D ZnO nanostructures which are basically monolayered nanofilms has seen an exponential surge [15-25]. According to Freemanm who originally predicted the potential existence of the monolayered ZnO (M-ZnO) phase, ZnO film tends to adopt a graphene-like structure when the number of layers is considerably diminished [15,16]. Tusche et *al*. [17] were the pioneering researchers to successfully synthesize a monolayered ZnO nanofilm on a Ag (111) substrate, where the Zn and O atoms organized themselves into a hexagonal thin nanosheet. The existence of ZnO nanosheet was later ascertained by Weirum et *al* [18] who grew graphene-like thin films on Pd (111) surface. Across the various studies, M-ZnO, similar to its bulk counterparts, has been reported to exhibit a direct wide band gap and paramagnetic characteristics, which in turn influence the optical properties of ZnO. Transition metals [19-21], non-metals [22,23] and trivalent cations [24-27] have been utilized as active dopants and reported to significantly boost electrical conductivity of ZnO. As a result, carrier recombination is remarkably suppressed yielding into a higher PCE in DSSC's.

* Corresponding author:
kahuramoses1234@gmail.com (Irungu M. Kahura)
Received: Oct. 28, 2024; Accepted: Nov. 19, 2024; Published: Nov. 22, 2024
Published online at http://journal.sapub.org/nn

The incorporation of rare earth metals as dopants in a ZnO host matrix has been extensively explored in various studies, with the objective of enhancing the electrical and optical properties. [28-38]. Vettumperumal et. *al* [28] prepared Erbium (Er) doped ZnO thin films using the solgel process and deposited them on a glass substrate via spin coating method. From their study, at low dopant concentration, the hexagonal lattice structure of wurtzite ZnO (W-ZnO) is preserved although at a stronger excitonic bond. As reported by da Fonseca et *al*., the integration of Europium (Eu) into the ZnO lattice down shift the conduction band (CB), ultimately resulting in a narrowed band gap [30]. This facilitated photoelectron injection from the dye to the CB of Eu-doped ZnO thereby elevating the DSSC PCE. The reduction in band gap accompanied with a red shift of absorption edge on RE doped ZnO was confirmed by Chamanzadeh et. *al* [31]. They investigated La and Dy doped ZnO nanorods synthesized via hydrothermal technique. Based on their findings, this approach resulted in a 3.8% improvement in the operational performance of DSSC. Utilizing first principle techniques, Khuilli et *al*. [35] conducted a theoretical investigation into the impact of doping ZnO with rare earth (RE) elements (Tb, Yb, and Ce) on its structural, magnetic, optoelectronic, and electrical properties. Contrary to other experimental and theoretical studies, the results indicated that RE doping broadened the band gap, which in turn produced a blue shift in the absorption edges. RE doping introduces a peculiar localized band between the CB and VB, a phenomenon attributed to the inclusion of the 4f orbital within the ZnO structure [31,38]. Furthermore, the 4f orbital is effectively shielded by the 5p and 5s orbitals, rendering the effects of temperature and crystal field on the 4f orbital minimal. This yields not only to rapid magnetic transformation, enhanced electrical conductivity but their optical transition even at strong electric field is highly stable [36].

From the above discussion, numerous reports on the structural, magnetic, electrical and optical properties of bulk ZnO doped with RE exist in literature. However, very little is known on the material properties of 2D M- ZnO doped with RE despite its promising applicability in DSSSC's. Specifically, a report on the optical properties of RE (Ce, Dy and Eu) doped M-ZnO is lacking in literature. The aim of this study is to improve on the electronic, electrical and optical properties of M-ZnO while maintaining its structural formation. To achieve this, a comparative study on structural, electronic, electrical and optical properties of M-ZnO doped with three RE elements: cerium (Ce), Dysprosium (Dy) and Europium (Eu) by use of density functional theorem (DFT) was conducted. To reproduce experimental accuracy on the electronic and optical calculations, GGA+U [39-46] was utilized in this study.

2. Computational Details

In this research, the crystal structure was derived from Material Project [47], and DFT calculations were subsequently performed using the Quantum ESPRESSO (QE) code [48]. The projector-augmented plane wave (PAW) with generalized gradient approximation by Perdew-Burke-Ernzerhof (GGA-PBE) [49] was employed in solving the Kohn-Sham equation [50]. A monolayer of ZnO (M-ZnO) comprising of 32 atoms was cleaved from a bulk wurtzite ZnO supercell. RE (Ce, Dy, Eu) doped M-ZnO models were then developed by substituting one Zn atom with one RE (Ce, Dy and Eu) atom. This translated to 2.78% dopant concentration which was low enough to avoid structural deformation. Prior DFT investigations indicated that zigzag ZnO nanotubes exhibit greater stability compared to their armchair counterparts [51]. In the structural optimization, the Brillouin zone was integrated using a Monkhorst Pack scheme [52] employing a K-mesh of 4 x 4 x 1. The wave function and charge density were subjected to energy cut-offs of 50 Ry and 500 Ry, respectively, with a total energy convergence threshold specified at 10^{-8} Ry. To avoid superfluous interactions between adjacent monolayers, a vacuum space measuring 15 Å [21] in thickness was incorporated into the calculations along the non-periodic axis. An analysis on the electronic properties of the pure, and RE doped M-ZnO was conducted utilizing the DFT+U approximation techniques. An onsite columbic potential of U_d=10, Up=8, U_f =5 eV was applied to the Zn-3d, O-2p and RE- 4f respectively. This was necessary since GGA functionals have been reported to severely underestimate the energy band gaps. To evaluate the optical properties of the different structures, thermos-pw code [53] integrated with QE was employed. Additionally, BoltzTrap code [54,55] integrated with Quantum ESPRESSO was also utilized to conduct calculations on the electrical conductivity of the M-ZnO structures.

3. Results and Discussions

3.1. Structure of ZnO

The structural properties were explored by first optimizing the lattice parameters of bulk wurtzite (W)-ZnO structure as shown in figure 1 (a). Its unit cell comprises two zinc atoms located at the coordinates (1/3, 2/3, 0) and (2/3, 1/3, 1/2), along with two oxygen atoms positioned at (1/3, 2/3, u) and (2/3, 1/3, 1/2 + u). The W-ZnO crystal consists of two interpenetrating hexagonal close-packed (hcp) sub-lattices. Each of the hcp consists of one type of atom displaced with respect to each other along the threefold c-axis, by an internal parameter u of 0.375 (in an ideal wurtzite structure) [56]. The optimal lattice constants were a=b= 3.289 Å and c= 5.284 Å . This was in good agreement with other experimental [56] and DFT [57] studies. M- ZnO structure, consisting of a single zinc and a single oxygen atom, was subsequently cleaved from the optimized W-ZnO featuring a (0001) polar surface. To investigate on the effects of RE (Ce, Dy, Eu) doping, a 4 x 4 x1 supercell as presented in figure 1 (b) was modeled with 32 atoms from which one Zn atom was replaced with one RE atom. Figure 1 (c) shows the optimized RE (Ce, Dy, Eu) doped M-ZnO used in this study.

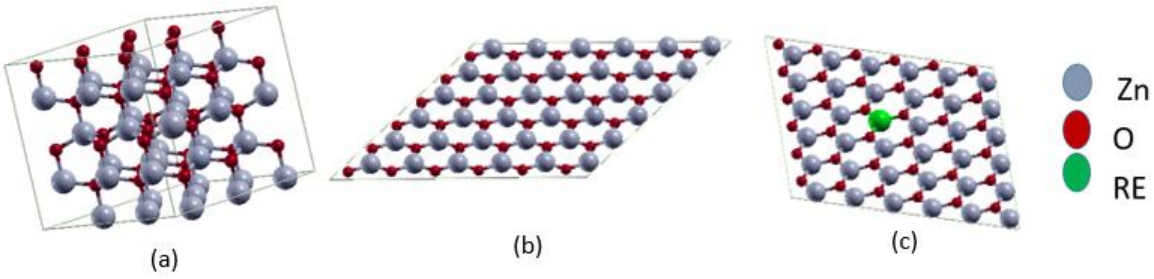

Figure 1. Schematic representation of (a) Bulk-ZnO supercell (b) pure M-ZnO supercell , (c) RE doped M-ZnO supercell structure using VESTA code [58]

After full relaxation, the bulk ZnO transforms from its original Wurtzite into a graphene-like planar structure [59]. The relaxed bond length of Zn-O in M-ZnO was measured by use of xcrysden code and observed to be 1.9102 Å Which collaborates well with experimental value of 1.92 Å [57] and other DFT value of 1.86 Å [60]. This bond length is shorter compared to that of bulk ZnO structure (2.01 Å). This contraction is linked to the sp2 hybridization in the honeycomb 2D framework of M-ZnO, which is stronger than the sp3 hybridization that occurs in W-ZnO [66]. The structure of RE-doped M-ZnO was then relaxed and it was observed that the honey-comb structure was well maintained as shown in figure 1c. The bond length of RE (Ce, Dy, Eu) to the nearest O atom was 2.18, 2.14 and 2.16 Å respectively. To the best of our knowledge there exist no reports on the lattice parameters and bond length of RE (Ce, Dy, Eu) doped M-ZnO to compare with.

Table 1. Optimized lattice constants a, bond length, bond angle in comparison with other studies of pure M-ZnO and RE doped M-ZnO

	Lattice parameter, a (Å)	Bond length (Å)	Bond angle (degree)	Reference
ZnO	3.289	1.91	120	This work
	3.264		120	Expt [56]
	3.214	1.92	120	DFT [57]
Ce:ZnO	3.314	2.18	120	This work
Dy:ZnO	3.319	2.14		This work
Eu:ZnO	3.324	2.16	120	This work

The computation of formation energies (E_f), as described in equation 1, was conducted for the RE-doped M-ZnO to ascertain their relative chemical stability.

$$E_f = E_{tot}(ZnO:RE) - E_{tot}(ZnO) + \mu_{zn} - \mu_{RE} \quad (1)$$

Where $E_{tot}(ZnO:RE)$ and $E_{tot}(ZnO)$ are the total energies per supercell of the relaxed RE doped and undoped ZnO respectively. The μ_{zn} and μ_{RE} represent the chemical potential of Zn and RE (Ce, Dy and Eu) respectively which is presumably the energy per atom in their respective metals. E_f is utilized as a stability metric, where a negative E_f indicates enhanced structural stability [61,62], thereby rendering the corresponding compound more desirable for experimental purposes. A plot of the obtained E_f is presented in figure 2 showing that the E_f of all RE doped M-ZnO tested was negative. This indicates that the doping process is thermodynamically and chemically favorable for each of these RE elements in the M- ZnO crystal lattice. The negative formation energy suggests that when Ce, Dy, or Eu atoms are incorporated into ZnO, the overall energy of the system decreases, making the RE doped M-ZnO structure more stable than the undoped ZnO.

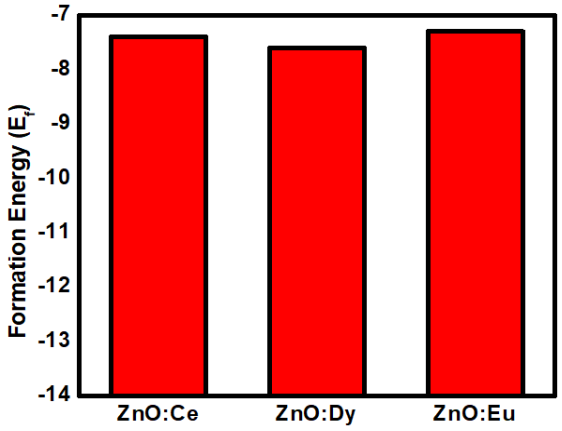

Figure 2. The formation energies of RE doped M-ZnO models

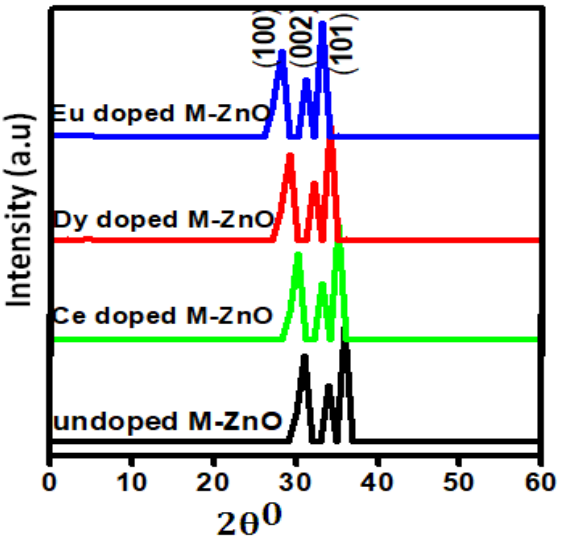

Figure 3. The XRD patterns for the undoped and RE (Ce, Dy, Eu) doped M-ZnO

This negative formation energy further implies that doping ZnO with Ce, Dy, or Eu does not require continuous energy input to maintain the stability of the doped structure, indicating that such materials can form naturally under suitable conditions. This is thereby an indication that Ce, Eu and Dy are suitable dopants into a ZnO monolayer matrix

with Dy being most favorable.

Upon optimizing the geometrical structures, we employed the VESTA code [58] to simulate the X-ray diffraction (XRD) spectra in order to examine the growth orientations of these materials. The findings illustrated in Figure 3 indicate that the hexagonal configuration of M-ZnO remains intact following the addition of RE elements, with no emergence of secondary peaks or novel phases. This is largely because the dopants Ce, Dy, and Eu have ionic radii that are reasonably compatible with Zn^{2+} ions [63]. This allows the dopants to substitute into the ZnO lattice without causing significant structural distortion. The dopants may occupy Zn sites or exist interstitially [64] without disrupting the ZnO lattice framework, thereby retaining the hexagonal configuration. The XRD spectra indicate that the RE (Ce, Dy and Eu) doped M-ZnO exhibits a polycrystalline structure. In the monolayer ZnO, the main peaks correspond to the (100), (002), and (101) planes, typically found at approximately 2θ =31.7°, 34.4° and 36.2°, respectively. These peaks indicate the wurtzite hexagonal crystal structure of ZnO, even in a monolayer structure. However, in M-ZnO, these peaks are much broader and weaker than in the bulk ZnO due to limited layer thickness and smaller crystal domains. The angular positions of the major peaks in RE (Ce, Dy and Eu) doped M-ZnO shift towards lower angles. This alteration in peak positions validates the increase in the lattice parameters thereby leading to an expansion of the ZnO structures. When the larger RE ions replace Zn^{2+} ions or occupy interstitial sites in the ZnO lattice, they cause a slight increase in lattice parameters. This expansion leads to an increase in the interplanar spacing, which results in a shift of X-ray diffraction (XRD) peaks toward lower angles according to Bragg's law [65]. The shift indicates successful incorporation of the dopants within the M-ZnO lattice.

3.2. Electronic Properties

To describe the electronic structure of our compounds, this study has computed the band structure, the partial as well as the total density of states of the RE (Ce, Dy and Eu) doped M-ZnO. The band gap is a critical parameter in DSSC material since it directly dictates the electrical conductivity and optical properties of a material [66]. The local density approximation (LDA) and GGA-PBE functional are commonly employed to address the electron-ion exchange correlation in the DFT formalism [67]. This would however lead to a severe band gap underestimation compared to experimental values due to the inadequacy of GGA functionals to treat the d and p hybridization. To rectify this shortcoming, a Hubbard U potential was introduced in the Zn-3d (10 eV) and O-2p (8 eV) and RE-4f (5eV) orbitals in the GGA+ U calculation [39-47]. Consequently, the band gap was widened to the experimental values of 3.38 eV as illustrated in figure 4(a) for the undoped M-ZnO. When M- ZnO is doped with RE (Ce, Dy, Eu), still the band gap was direct but narrowed down which is an important factor for optical performance in DSSC photoanode. As shown in figures 4 (b-d), the band structure is more compact indicating great interaction amongst the various atoms in the RE doped M-ZnO. The fermi level was noted to shift upwards towards the CB reflecting that RE (Ce, Dy, Eu) acts as donor dopant resulting into n-type extrinsic semiconductor due to Burstein-moss effect [68].

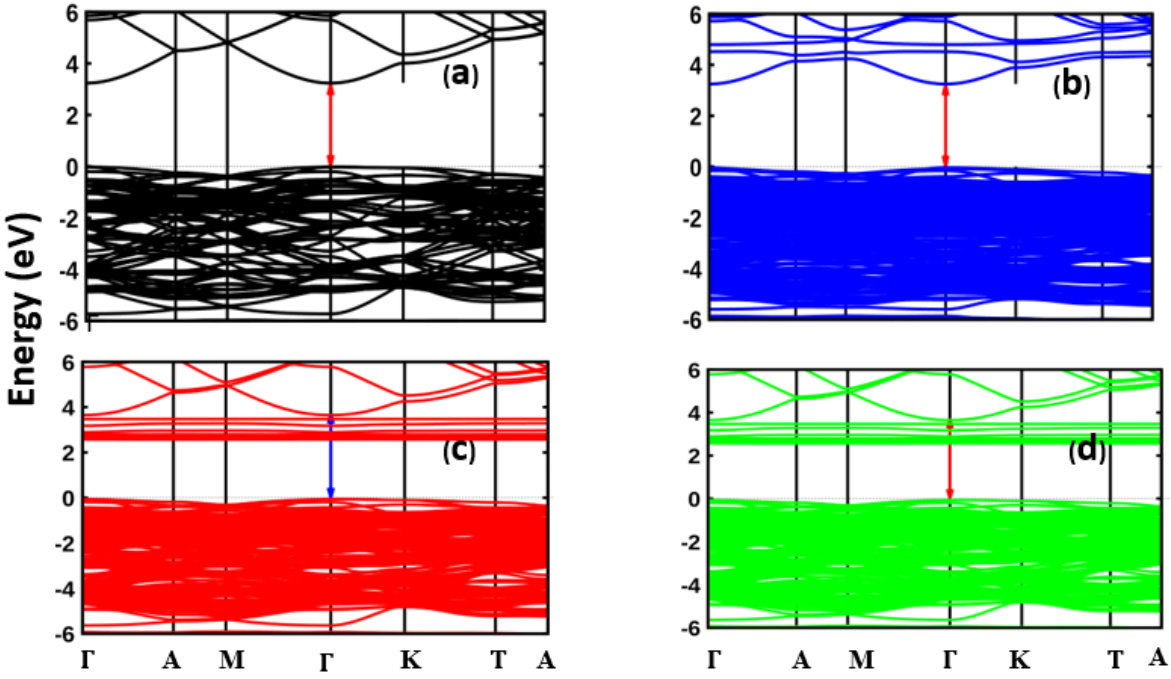

Figure 4. The electronic band structures of (a) pure (b) Ce doped, (c) Dy doped and (d) Eu doped M-ZnO

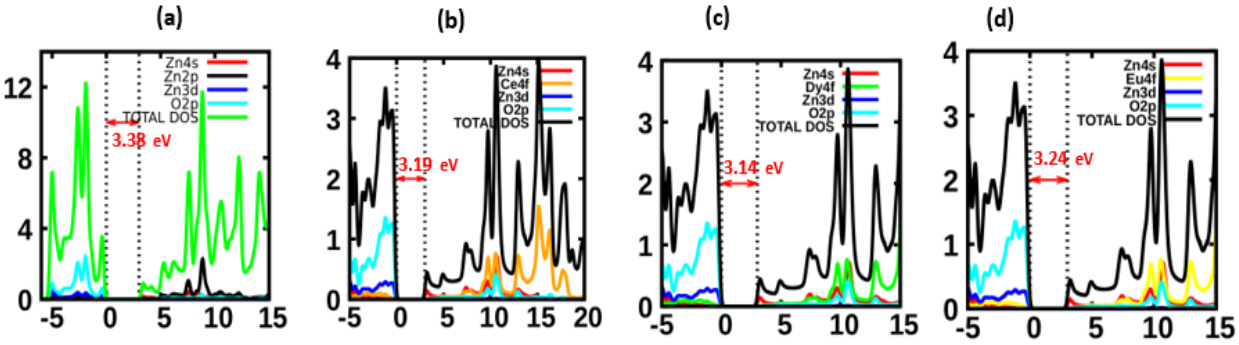

Figure 5. The total DOS and PDOS of (a) pure (b) Ce doped, (c) Dy doped and (d) Eu doped M-ZnO

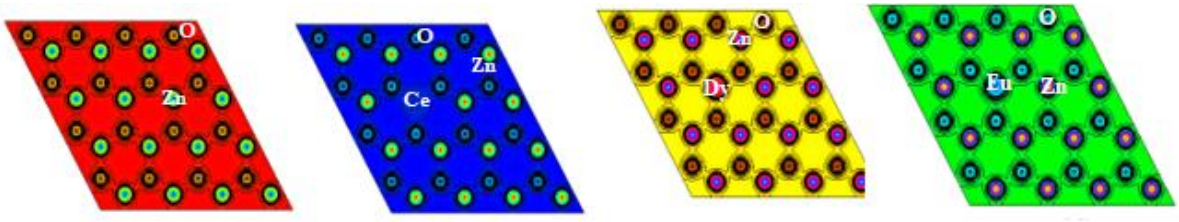

Figure 6. The electron density for the (a) pure (b) Ce doped, (c) Dy doped and (d) Eu doped M-ZnO

From the measurement of band gap the fermi level (set at zero) to the minimum of the CB, the band gap was found to decrease with RE doping. The values obtained were 3.19, 3.14 and 3.24 eV for Ce, Dy and Eu doped M-ZnO respectively. Substituting RE for Zn further generated isolated impurity bands located in the band gap region which was a unique feature in RE (Ce, Dy, Eu) doped M-ZnO. This was attributed to the 4f orbital introduced into the ZnO structure by the RE dopant atoms and is expected to enhance phonon absorption [69]. Positioned above the Fermi level, these isolated states further acts as a trampoline, facilitating the transition of electrons into the CB via thermal and photo-excitation mechanisms. This occurrence diminishes the necessity for photon energy and can promote movement of photogenerated charge carriers in DSSC's [70]. The study also performed an analysis of the DOS and PDOS to further interrogate the electronic properties of pure and RE (Ce, Dy and Eu) doped M-ZnO. It was found that the O-2s dominated the lower energy region (-18 eV) of the VB. The region near the fermi level was occupied by both the Zn-3d and O-2p orbitals whose hybridization generate a very strong Zn-O bond as shown in figure 5.

The CB of the pure M-ZnO is mainly dominated by the Zn-4s, and O-2p which is in strong agreement with other studies [71]. Upon RE doping, the valence states were clearly noted to shift towards the lower energy regions as shown in figure 5 (b-d). While the Zn-3d and O-2p dominated the VB, the RE-4f and O-2p orbitals were observed in the CB. The appearance of peculiar occupied states near the fermi level was observed. This was mainly derived from the contribution of the 4f orbital of the RE dopant, a feature that strongly affect the photoelectric characteristic of M-ZnO.

In order to assess the chemical bonds, present in the compounds, we have mapped their (110) electron density, illustrated in Figure 6.

The electron density offers insights into the distribution of charge within the unit cell of materials, enabling the identification of the types of chemical bonds that exist within these materials [72]. The results clearly illustrate that the RE–O bonds are chiefly characterized by ionic interactions. The almost spherical arrangement of electronic distribution around these atoms makes this evident. Therefore, it can be concluded that substituting Zn with an RE atom does not substantially change the bonding properties of these M-ZnO compounds [73].

3.3. Optical Properties

An appropriate compound for use in the photoanode of DSSC's should be selected with careful consideration of its optical properties. An analysis of the optical properties of pure M-ZnO and RE (Ce, Dy and Eu) doped M-ZnO was conducted within the photon energy spectrum of [0, 20] eV. Several investigations have shown that the complex dielectric function ε(ω), as outlined in Equation 2, is a crucial physical metric for assessing and characterizing the unique optical properties of a material [74].

$$\varepsilon(\omega) = \varepsilon_1(\omega) + i\varepsilon_2(\omega) \quad (2)$$

Where $\varepsilon_1(\omega)$ and $\varepsilon_2(\omega)$ are the real and complex parts respectively of the complex dielectric functions. While the real part, explains the photon dispersion and extent of material polarisation, the imaginary component describes the photon absorption of a material. The calculations of momentum matrix elements, as described in equation 3, yields the imaginary component when considering transitions between unoccupied and occupied wavefunctions $\varepsilon_2(\omega)$ [75].

$$\varepsilon_2(\omega) = \frac{8\pi^2 e^2}{\omega^2 m^2}$$

$$\sum_n \sum_{n'} \int |P^v_{nn'}(k)|^2 f_{kn}(1 - f_{nn'}) \delta\left(E^k_n - E^k_{n'} - \hbar\omega\right) \frac{d^3k}{(2\pi)^3} \quad (3)$$

The Kramer – Kronig relation given by equation (4) was used to derive the real part $\varepsilon_1(\omega)$ from $\varepsilon_2(\omega)$ [75].

$$\varepsilon_1(\omega) = 1 + \frac{2}{\pi}\int_0^\infty \frac{\varepsilon_2(\omega)\omega' d\omega'}{\omega'^2 - \omega^2} \quad (4)$$

The extraction of other optical constants, including the absorption coefficient α(ω), refractive index n(ω), energy loss spectrum L(ω), and reflectivity R(ω) was performed using $\varepsilon_1(\omega)$ and $\varepsilon_2(\omega)$ as described in equations 5-8.

$$\alpha(\omega) = \sqrt{2\omega}\left(\sqrt{\varepsilon_1{}^2(\omega) + \varepsilon_2{}^2(\omega)} - \varepsilon_1(\omega)\right)^{\frac{1}{2}} \quad (5)$$

$$n(\omega) = \frac{1}{\sqrt{2}}\left(\frac{\sqrt{\varepsilon_1{}^2(\omega) + \varepsilon_2{}^2(\omega)} + \varepsilon_1(\omega)}{2}\right)^{\frac{1}{2}} \quad (6)$$

$$L(\omega) = \frac{\varepsilon_2(\omega)}{\varepsilon_1{}^2(\omega) + \varepsilon_2{}^2(\omega)} \quad (7)$$

$$R(\omega) = \frac{(n-1)^2 + K^2}{(n+1)^2 + K^2} \quad (8)$$

Figure 7 and 8 represents the optical graphs as a function of energy in eV. In Figure 7(a), the electronic aspect of the calculated dielectric function, denoted as $\varepsilon_1(0)$ is presented for pure M-ZnO alongside RE (Ce, Dy and Eu) doped M-ZnO. As demonstrated in Table 2, the refractive indices were derived by applying the square root to these values [74]. From this table, the Dy doped M-ZnO has the highest $\varepsilon_1(0)$ as well as the refractive index. The imaginary spectrum characterizes the correlation between the optical and electronic attributes of a given material. From figure 7(b) of $\varepsilon_2(\omega)$ as a function of energy, the critical onset points are located at 3.37, 3.18,3.15 and 3.24 eV for pure, Ce, Dy and Eu doped M-ZnO compounds respectively. The values are consistent with the energy band gaps derived from band structure calculations. Three main peaks at approximately 5.2, 8.1 and 15.5 eV for all the compounds tested were observed on $\varepsilon_2(\omega)$ plot resulting from the transition of an electron from the valence to the conduction band. The absorption coefficient reflects the extent to which light intensity declines per unit distance in a material medium. The photon frequency significantly influences this parameter, indicating that the incident photon interacts with the electrons within the material, which facilitates inter-band transition from the valence to conduction bands. According to Figure 7(c), absorption edge of M-ZnO was observed at 3.38, 3.185, 3.15 and 3.23 eV for the pure, Ce, Dy and Eu doped M-ZnO compounds respectively as presented in Table 2. The analysis shows that M-ZnO allows the majority of visible light of the solar radiation to pass through, which is a critical requirement for its function as a photoanode in DSSCs. Therefore, M-ZnO effectively transmits light to the absorption dye, enabling photoemission and the generation of electrical current [76].

The Refractive index of an optical medium is a dimensionless quantity that describes the bending of a beam through that medium [74]. Materials of considerably high refractive index (above 2.0) are desired in photovoltaic applications. The calculated refractive index of M-ZnO is displayed in the plot of Figure 8(a) and the results are presented in Table 2. The static refractive indices from all the compounds are high enough for the application of M-ZnO in a DSSC photoanode. A significant decay in the dispersion curve of the refractive index was observed after the first peak indicating that beyond a certain amount of photon energy, M-ZnO fails to maintain its transparent nature and instead absorbs such radiations. Reflectivity depicts the surface behavior of a material. Figure 8(b) shows a low reflectivity at zero photon energy (R_0). The least reflectivity was observed in Eu doped M-ZnO implying its ability to reflect minimum solar radiation but instead allow it to pass through for dye excitation in DSSC. From the plot, the highest peaks are observed at approximately 10-15 eV after which the reflectivity starts to drop. Energy loss L (ω) is another vital parameter that characterizes the loss of energy of a fast-moving electron as it transverses a material medium. Figure 8(c) shows a near zero energy loss up to 4.0 eV in all the tested compounds. At higher photon energy, the energy loss in M-ZnO gradually rises to a peak at 5.5 eV. The capability of M-ZnO within UV-Vis region to retain most of its energy with negligible energy loss to the surrounding as desired in DSSCs photoanode is therefore confirmed. However, for high-energy radiations, the energy loss of M-ZnO is relatively high.

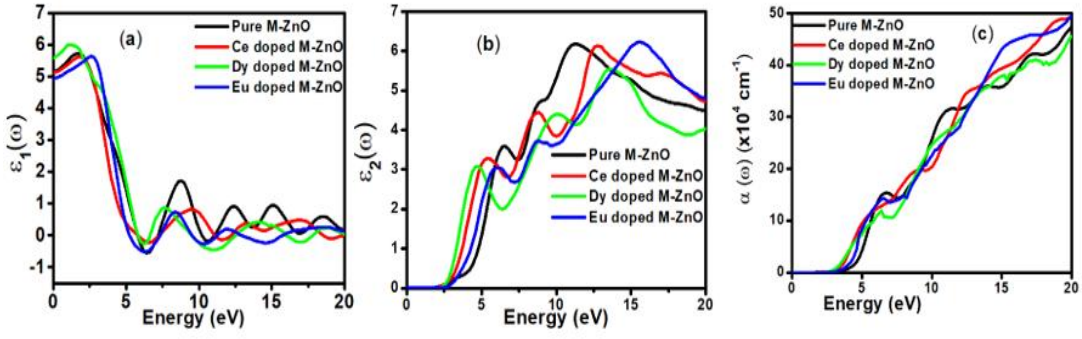

Figure 7. The (a) real part and (b) imaginary part of the dielectric constant, (c) absorption coefficient of the pure and RE (Ce, Dy, Eu) doped M-ZnO

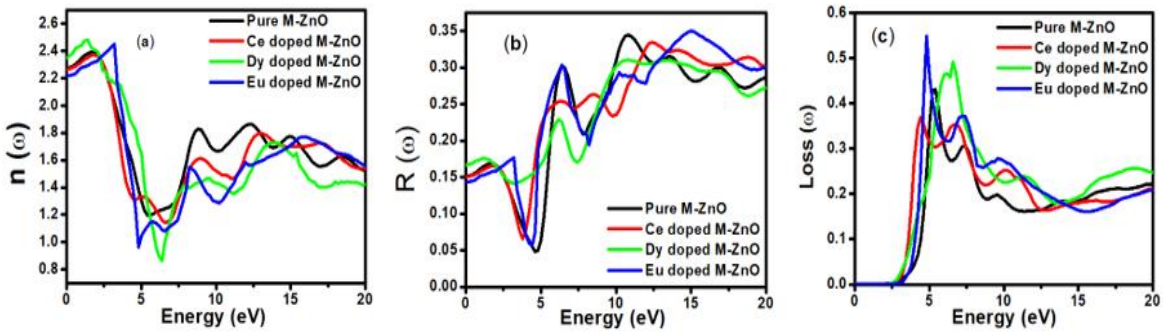

Figure 8. The (a)refractive index, (b) reflectivity and (c) energy loss as a function of the energy in eV for the pure and RE (Ce, Dy, Eu) doped M-ZnO

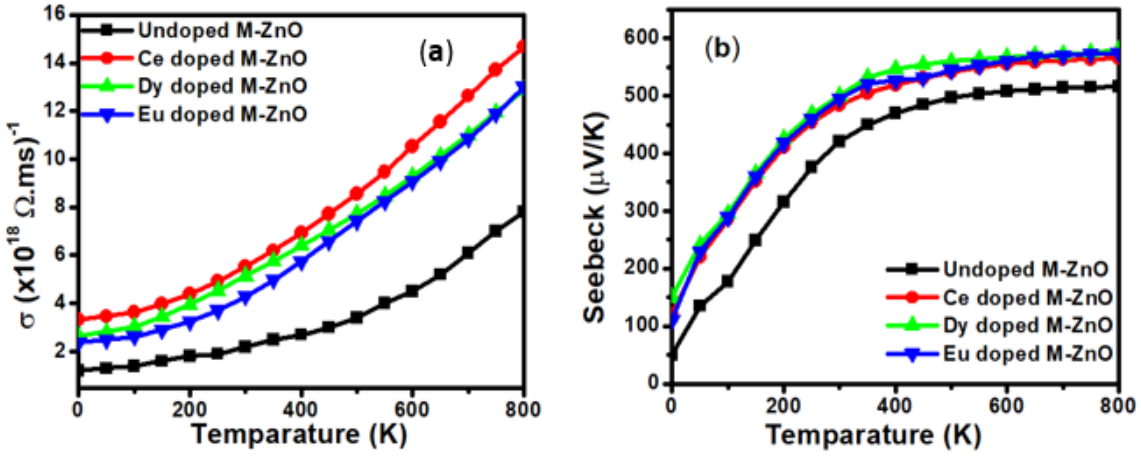

Figure 9. The (a) Electrical conductivity and (b) Seebeck coefficient of undoped and RE (Ce, Dy and Eu) doped M-ZnO

Table 2. Real dielectric function at 0 eV{$\varepsilon_1(0)$}, refractive index (n), absorption critical points and reflectivity at 0 eV (R_0)

	$\varepsilon_1(0)$	Refractive index	Absorption critical points	R(0)
Undoped	5.1	2.30	3.38	0.150
Ce doped M-ZnO	5.05	2.29	3.185	0.156
Dy doped M-ZnO	5.5	2.38	3.15	0.174
Eu doped M-ZnO	4.98	2.21	3.23	0.148

3.4. Electrical Properties

Relative to other metal oxide semiconductors applied in DSSC, ZnO exhibits superior electrical conductivity and lower resistivity [35]. This analysis entails the evaluation and comparison of the electrical conductivity of pure M-ZnO and RE (Ce, Dy, Eu) doped M-ZnO. To affirm the validity of our results, we also report the Seebeck coefficients, which serve to illustrate the inverse correlation between the electrical conductivity coefficients and the seebeck coefficients. To derive these transport coefficients, the semi-classical Boltzmann transport equations were addressed under the constant relaxation time approximation, utilizing the BoltzTraP code [55] for execution.

The electrical conductivity is described by equation 9 [35].

$$\sigma_{\alpha\beta}\ (T,\mu) = \frac{1}{\Omega}\int \sigma_{\alpha\beta}\,(\varepsilon)\left[-\frac{\partial f_\mu\,(T,\varepsilon)}{\partial\varepsilon}\right]d\varepsilon \qquad (9)$$

Where $\sigma_{\alpha\beta}$ is the conductivity tensor given by equation 10, Ω is the volume of unit cell and f_μ is the fermi distribution.

$$\sigma_{\alpha\beta}\ (i,k) = e^2\tau_{i,k}V_\alpha(i,k)V_\beta(i,k) \qquad (10)$$

Where τ is the electronic relaxation time designating the time interval between two successive collisions of charge carriers. V_α and V_β represent the velocities of charge carries in the corresponding directions $\alpha\ and\ \beta$ respectively. Figure 9(a) shows the computed electrical conductivity in relation to changes in temperature. The figure demonstrates that there is a direct correlation between the electrical conductivity of ZnO and temperature across all compounds that were tested. This is attributed to the enhanced concentration of charge carriers in the conduction band that accompanies a rise in temperature. In terms of conductivity, the Ce doped M-ZnO outperformed all other materials evaluated. Utilizing this high conductivity within DSSC is projected to diminish the electron-hole recombination, consequently enhancing the PCE of the solar cell.

The Seebeck coefficient of M- ZnO vary significantly from that of bulk ZnO due to quantum confinement, altered electronic structure, and a reduced dimensionality effect. Its notable from Figure 9(b) that the seebeck coefficient increased with temperature. This can be attributed to enhanced scattering effects and more pronounced energy filtering. The seebeck coefficient observed in this study attained peak values at 516, 565.7, 580 and 574 $\mu V/K$ at 800 K for pure

M-ZnO and RE (Ce, Dy, Eu) doped M-ZnO respectively as shown in Table 3. Among the materials tested, Dy doped M-ZnO had the highest seebeck coefficient of 580 μV/K at 800K depicting it as the best thermoelectric structure. Based on reports from previous studies, materials with seebeck coefficient above 200 μV/K are considered good thermoelectric compounds [77]. The seebeck coefficient values obtained in this study were higher than 200 μV/K ascertaining pure and RE (Ce, Dy, Eu) doped M-ZnO as viable thermoelectric compound especially at elevated temperatures. RE-doped M-ZnO show modified electrical conductivity and an enhanced Seebeck coefficient. The introduction of RE ions introduce localized states that facilitate charge carrier movement, improving thermoelectric efficiency. RE doping also improve carrier concentration, consequently reducing the resistivity of M-ZnO, particularly in n-type configurations.

Table 3. Transport coefficients of ZnO at different temperatures

Thermoelectric coefficient	Undoped -ZnO	Ce-ZnO	Dy-ZnO	Eu-ZnO
S (μV/K)				
200K	315.4	411.6	426	418
400K	470	518.8	547	527
600K	508.6	554.4	567	560
800K	516	565.7	580	574
σ (x 10^{18} S/ms)				
200K	1.8	4.4	4.0	3.3
400K	2.7	6.93	6.39	5.75
600K	4.5	10.54	9.3	9.07
800K	7.8	14.7	12.9	13.01

4. Conclusions

This work presents an analysis of the effects of doping M-ZnO with RE (Ce, Dy, Eu) employing DFT+U. The findings indicated that the introduction of these elements into M-ZnO at low concentrations preserves the hexagonal symmetry inherent to M-ZnO structure**.** Additionally, there is an observed increase in the lattice parameters, which aligns well with the experimental findings. The electronic architecture of the doped systems illustrates the localization of the 4f states across the various forms of RE doped M-ZnO. This significantly influences their optical and electrical characteristics, thereby imparting essential properties to RE-doped M-ZnO that are favorable for application in DSSCs. The incorporation of RE (Ce, Dy, Eu) into M-ZnO resulted in minimal absorption and reflectivity levels below 7% within the visible spectrum. Doping M-ZnO with RE (Ce, Dy, Eu) resulted into a red shift in the absorption edge indicating a reduction in the band gap relative to that of pure M-ZnO. Additionally, it is noted that there has been an improvement in electrical conductivity subsequent to the doping. The research results reveal that RE (Ce, Dy, Eu) -doped M-ZnO is a viable material for implementation in DSSC technology.

REFERENCES

[1] Repins, I., Contreras, M. A., Egaas, B., DeHart, C., Scharf, J., Perkins, C. L., ... & Noufi, R. (2008). 19· 9%-efficient ZnO/CdS/CuInGaSe2 solar cell with 81· 2% fill factor. *Progress in Photovoltaics: Research and applications*, *16*(3), 235-239.

[2] Tsukazaki, A., Ohtomo, A., Onuma, T., Ohtani, M., Makino, T., Sumiya, M., ... & Kawasaki, M. (2005). Repeated temperature modulation epitaxy for p-type doping and light-emitting diode based on ZnO. *Nature materials*, *4*(1), 42-46.

[3] Lee, K. M., Lai, C. W., Ngai, K. S., & Juan, J. C. (2016). Recent developments of zinc oxide based photocatalyst in water treatment technology: a review. *Water research*, *88*, 428-448.

[4] Chen, X., Wu, Z., Liu, D., & Gao, Z. (2017). Preparation of ZnO photocatalyst for the efficient and rapid photocatalytic degradation of azo dyes. *Nanoscale research letters*, *12*, 1-10.

[5] Ouyang, W., Chen, J., Shi, Z., & Fang, X. (2021). Self-powered UV photodetectors based on ZnO nanomaterials. *Applied physics reviews*, *8*(3).

[6] Patel, M., Song, J., Kim, D. W., & Kim, J. (2022). Carrier transport and working mechanism of transparent photovoltaic cells. *Applied Materials Today*, *26*, 101344.

[7] Lu, L., Li, R., Fan, K., & Peng, T. (2010). Effects of annealing conditions on the photoelectrochemical properties of dye-sensitized solar cells made with ZnO nanoparticles. *Solar Energy*, *84*(5), 844-853.

[8] Lyons, J. L., Janotti, A., & Van de Walle, C. G. (2009). Why nitrogen cannot lead to p-type conductivity in ZnO. *Applied Physics Letters*, *95*(25).

[9] Zhang, Y. G., Zhang, G. B., & Xu Wang, Y. (2011). First-principles study of the electronic structure and optical properties of Ce-doped ZnO. *Journal of Applied Physics*, *109*(6).

[10] Ungula, J., Kiprotich, S., Swart, H. C., & Dejene, B. F. (2022). Investigation on the material properties of ZnO nanorods deposited on Ga-doped ZnO seeded glass substrate: Effects of CBD precursor concentration. *Surface and Interface Analysis*, *54*(10), 1023-1031.

[11] Ungula, J. (2015). *Growth and characterization of ZnO nanoparticles by sol-gel process* (Doctoral dissertation, University of the Free State (Qwaqwa Campus)).

[12] Aksoy, S., Polat, O., Gorgun, K., Caglar, Y., & Caglar, M. (2020). Li doped ZnO based DSSC: Characterization and preparation of nanopowders and electrical performance of its DSSC. *Physica E: Low-dimensional Systems and Nanostructures*, *121*, 114127.

[13] Lin, C. Y., Lai, Y. H., Chen, H. W., Chen, J. G., Kung, C. W., Vittal, L. R., & Ho, K. C. (2011). Highly efficient dye-sensitized solar cell with a ZnO nanosheet-based photoanode. *Energy & Environmental Science*, *4*(9), 3448-3455.

[14] Quintana, M., Edvinsson, T., Hagfeldt, A., & Boschloo, G. (2007). Comparison of dye-sensitized ZnO and TiO2 solar cells: studies of charge transport and carrier lifetime. *The Journal of Physical Chemistry C*, *111*(2), 1035-1041.

[15] Freeman, C. L., Claeyssens, F., Allan, N. L., & Harding, J. H. (2006). Graphitic nanofilms as precursors to wurtzite films: theory. *Physical review letters*, *96*(6), 066102.

[16] Freeman, C. L., Claeyssens, F., Allan, N. L., & Harding, J. H. (2006). Graphitic nanofilms as precursors to wurtzite films: theory. *Physical review letters*, *96*(6), 066102.

[17] Tusche, C., Meyerheim, H. L., & Kirschner, J. (2007). Observation of depolarized ZnO (0001) monolayers: formation of unreconstructed planar sheets. *Physical review letters*, *99*(2), 026102.

[18] Weirum, G., Barcaro, G., Fortunelli, A., Weber, F., Schennach, R., Surnev, S., & Netzer, F. P. (2010). Growth and surface structure of zinc oxide layers on a Pd (111) surface. *The Journal of Physical Chemistry C*, *114*(36), 15432-15439.

[19] He, A. L., Wang, X. Q., Wu, R. Q., Lu, Y. H., & Feng, Y. P. (2010). Adsorption of an Mn atom on a ZnO sheet and nanotube: A density functional theory study. *Journal of Physics: Condensed Matter*, *22*(17), 175501.

[20] Schmidt, T. M., Miwa, R. H., & Fazzio, A. (2010). Ferromagnetic coupling in a Co-doped graphenelike ZnO sheet. *Physical Review B*, *81*(19), 195413.

[21] Ren, J., Zhang, H., & Cheng, X. (2013). Electronic and magnetic properties of all 3d transition-metal-doped ZnO monolayers. *International Journal of Quantum Chemistry*, *113*(19), 2243-2250.

[22] Zheng, F. B., Zhang, C. W., Wang, P. J., & Luan, H. X. (2012). First-principles prediction of the electronic and magnetic properties of nitrogen-doped ZnO nanosheets. *Solid state communications*, *152*(14), 1199-1202.

[23] Guo, H., Zhao, Y., Lu, N., Kan, E., Zeng, X. C., Wu, X., & Yang, J. (2012). Tunable magnetism in a nonmetal-substituted ZnO monolayer: a first-principles study. *The Journal of Physical Chemistry C*, *116*(20), 11336-11342.

[24] Zhang, W. X., T. Li, C. He, X. L. Wu, L. Duan, H. Li, L. Xu, and S. B. Gong. "First-principle study on Ag-2N heavy codoped of p-type graphene-like ZnO nanosheet." *Solid State Communications* 204 (2015): 47-50.

[25] Ungula, J. (2018). *Formation and characterization of novel nanostructured un-doped and Ga-doped ZnO transparent conducting thin films for photoelectrode* (Doctoral dissertation, University of the Free State (Qwaqwa Campus)).

[26] Omidvar, A. (2018). Indium-doped and positively charged ZnO nanoclusters: versatile materials for CO detection. *Vacuum*, *147*, 126-133.

[27] Khuili, M., El Hallani, G., Fazouan, N., Abou El Makarim, H., & Atmani, E. H. (2019). First-principles calculation of (Al, Ga) co-doped ZnO. *Computational Condensed Matter*, *21*, e00426.

[28] Vettumperumal, R., Kalyanaraman, S., & Thangavel, R. (2015). Optical constants and near infrared emission of Er doped ZnO sol–gel thin films. *Journal of Luminescence*, *158*, 493-500.

[29] Tan, C., Xu, D., Zhang, K., Tian, X., & Cai, W. (2016). Electronic and magnetic properties of rare-earth metals doped ZnO monolayer. *Journal of Nanomaterials*, *16*(1), 356-356.

[30] da Fonseca, A. F. V., Siqueira, R. L., Landers, R., Ferrari, J. L., Marana, N. L., Sambrano, J. R., ... & Schiavon, M. A. (2018). A theoretical and experimental investigation of Eu-doped ZnO nanorods and its application on dye sensitized solar cells. *Journal of Alloys and Compounds*, *739*, 939-947.

[31] Chamanzadeh, Z., Ansari, V., & Zahedifar, M. (2021). Investigation on the properties of La-doped and Dy-doped ZnO nanorods and their enhanced photovoltaic performance of Dye-Sensitized Solar Cells. *Optical Materials*, *112*, 110735.

[32] Tan, C., Xu, D., Zhang, K., Tian, X., & Cai, W. (2016). Electronic and magnetic properties of rare-earth metals doped ZnO monolayer. *Journal of Nanomaterials*, *16*(1), 356-356.

[33] Mary, J. A., Vijaya, J. J., Dai, J. H., Bououdina, M., Kennedy, L. J., & Song, Y. (2015). Experimental and DFT studies of structure, optical and magnetic properties of (Zn1− 2xCexCox) O nanopowders. *Journal of Molecular Structure*, *1084*, 155-164.

[34] Wen, J. Q., Zhang, J. M., Chen, G. X., Wu, H., & Yang, X. (2018). The structural, electronic and optical properties of Nd doped ZnO using first-principles calculations. *Physica E: Low-dimensional Systems and Nanostructures*, *98*, 168-173.

[35] Khuili, M., Fazouan, N., Abou El Makarim, H., Atmani, E. H., Rai, D. P., & Houmad, M. (2020). First-principles calculations of rare earth (RE= Tm, Yb, Ce) doped ZnO: Structural, optoelectronic, magnetic, and electrical properties. *Vacuum*, *181*, 109603.

[36] Nekvindova, P., Cajzl, J., Mackova, A., Malinský, P., Oswald, J., Boettger, R., & Yatskiv, R. (2020). Er implantation into various cuts of ZnO–experimental study and DFT modelling. *Journal of Alloys and Compounds*, *816*, 152455.

[37] Zhang, F., Gan, Q., Yan, M., Cui, H., Zhang, H., Chao, D., ... & Zhang, W. (2016). The first-principles study of electronic structures, magnetic and optical properties for Ce-doped ZnO. *Integrated Ferroelectrics*, *172*(1), 87-96.

[38] Wen, J. Q., Han, Y. S., Yang, X., & Zhang, J. M. (2019). Computational research of electronic, optical and magnetic properties of Ce and Nd co-doped ZnO. *Journal Of Physics And Chemistry Of Solids*, *125*, 90-95.

[39] Mulwa, W. M., Ouma, C. N., Onani, M. O., & Dejene, F. B. (2016). Energetic, electronic and optical properties of lanthanide doped TiO2: An ab initio LDA+ U study. *Journal of Solid State Chemistry*, *237*, 129-137.

[40] Agapito, L. A., Curtarolo, S., & Nardelli, M. B. (2015). Reformulation of DFT+ U as a pseudohybridhubbard density functional for accelerated materials discovery. *Physical Review X*, *5*(1), 011006.

[41] Deng, X. Y., Liu, G. H., Jing, X. P., & Tian, G. S. (2014). On-site correlation of p-electron in d10 semiconductor zinc oxide. *International Journal of Quantum Chemistry*, *114*(7), 468-472.

[42] Harun, K., Salleh, N. A., Deghfel, B., Yaakob, M. K., & Mohamad, A. A. (2020). DFT+ U calculations for electronic, structural, and optical properties of ZnO wurtzite structure: A review. *Results in Physics*, *16*, 102829.

[43] S.L. Dudarev, G.A. Botton, S.Y. Savrasov, C.J. Humphreys, A.P. Sutton, Electron-energy-loss spectra and the structural stability of nickel oxide: An LSDA+U study, Phys. Rev. B. 57 (1998) 1505–1509.

[44] Cococcioni, M., & De Gironcoli, S. (2005). Linear response approach to the calculation of the effective interaction parameters in the LDA+ U method. *Physical Review B*, *71*(3), 035105.

[45] Ma, X., Wu, Y., Lv, Y., & Zhu, Y. (2013). Correlation effects on lattice relaxation and electronic structure of ZnO within the GGA+ U formalism. *The Journal of Physical Chemistry C*, *117*(49), 26029-26039.

[46] Huang, G. Y., Wang, C. Y., & Wang, J. T. (2012). Detailed check of the LDA+ U and GGA+ U corrected method for defect calculations in wurtzite ZnO. *Computer Physics Communications*, *183*(8), 1749-1752.

[47] Jain, A., Montoya, J., Dwaraknath, S., Zimmermann, N. E., Dagdelen, J., Horton, M., ... & Persson, K. (2020). The materials project: Accelerating materials design through theory-driven data and tools. *Handbook of Materials Modeling: Methods: Theory and Modeling*, 1751-1784.

[48] Giannozzi, P., Baroni, S., Bonini, N., Calandra, M., Car, R., Cavazzoni, C., &Wentzcovitch, R. M. (2009). QUANTUM ESPRESSO: a modular and open-source software project for quantum simulations of materials. *Journal of physics: Condensed matter*, *21*(39), 395502.

[49] Perdew, J. P., Burke, K., & Ernzerhof, M. (1996). Generalized gradient approximation made simple. *Physical review letters*, *77*(18), 3865.

[50] Kohn, W., & Sham, L. J. (1965). Self-consistent equations including exchange and correlation effects. *Physical review*, *140*(4A), A1133.

[51] Solola, G. T., Bamgbose, M. K., Adebambo, P. O., Ayedun, F., & Adebayo, G. A. (2023). First-principles investigations of structural, electronic, vibrational, and thermoelectric properties of half-Heusler VYGe (Y= Rh, Co, Ir) compounds. *Computational Condensed Matter*, e00827.

[52] Monkhorst, H. J., & Pack, J. D. (1976). Special points for Brillouin-zone integrations. *Physical review B*, *13*(12), 5188-5192.

[53] Motornyi, O., Raynaud, M., Dal Corso, A., & Vast, N. (2018, December). Simulation of electron energy loss spectra with the turboEELS and thermo_pw codes. In *Journal of Physics: Conference Series* (Vol. 1136, No. 1, p. 012008). IOP Publishing.

[54] Litim, D. F., & Manuel, C. (2002). Semi-classical transport theory for non-Abelian plasmas. *Physics reports*, *364*(6), 451-539.

[55] Madsen, G. K., & Singh, D. J. (2006). BoltzTraP. A code for calculating band-structure dependent quantities. *Computer Physics Communications*, *175*(1), 67-71.

[56] Topsakal, M., Cahangirov, S., Bekaroglu, E., & Ciraci, S. (2009). First-principles study of zinc oxide honeycomb structures. *Physical Review B*, *80*(23), 235119.

[57] Tan, C., Sun, D., Xu, D., Tian, X., & Huang, Y. (2016). Tuning electronic structure and optical properties of ZnO monolayer by Cd doping. *Ceramics International*, *42*(9), 10997-11002.

[58] Momma, K., & Izumi, F. (2011). VESTA 3 for three-dimensional visualization of crystal, volumetric and morphology data. *Journal of applied crystallography*, *44*(6), 1272-1276.

[59] Fang, D. Q., Rosa, A. L., Zhang, R. Q., & Frauenheim, T. (2010). Theoretical exploration of the structural, electronic, and magnetic properties of ZnO nanotubes with vacancies, antisites, and nitrogen substitutional defects. *The Journal of Physical Chemistry C*, *114*(13), 5760-5766.

[60] Tu, Z. C. (2010). First-principles study on physical properties of a single ZnO monolayer with graphene-like structure. *Journal of Computational and Theoretical Nanoscience*, *7*(6), 1182-1186.

[61] Tan, C., Sun, D., Tian, X., & Huang, Y. (2016). First-principles investigation of phase stability, electronic structure and optical properties of MgZnO monolayer. *Materials*, *9*(11), 877.

[62] Haq, B. U., AlFaify, S., Alrebdi, T. A., Ahmed, R., Al-Qaisi, S., Taib, M. F. M., ... & Zahra, S. (2021). Investigations of optoelectronic properties of novel ZnO monolayers: A first-principles study. *Materials Science and Engineering: B*, *265*, 115043.

[63] Abderrahmane, B., Djamila, A., Chaabia, N., & Fodil, R. (2020). Improvement of ZnO nanorods photoelectrochemical, optical, structural and morphological characterizations by cerium ions doping. *Journal of Alloys and Compounds*, *829*, 154498.

[64] Ullah Awan, S., Hasanain, S. K., Bertino, M. F., & Hassnain Jaffari, G. (2012). Ferromagnetism in Li doped ZnO nanoparticles: The role of interstitial Li. *Journal of Applied Physics*, *112*(10).

[65] Bett, K., & Kiprotich, S. (2024). Effects of Stirring Speed of Precursor Solution on the Structural Optical and Morphological Properties of ZnO Al Ga CoDoped Nanoparticles Synthesized via a Facile Sol Gel Technique.

[66] Ungula, J. (2015). *Growth and characterization of ZnO nanoparticles by sol-gel process* (Doctoral dissertation, University of the Free State (Qwaqwa Campus)).

[67] Jantrasee, S., Moontragoon, P., & Pinitsoontorn, S. (2016). Thermoelectric properties of Al-doped ZnO: experiment and simulation. *Journal of Semiconductors*, *37*(9), 092002.

[68] Papadimitriou, D. N. (2022). Engineering of optical and electrical properties of electrodeposited highly doped Al: ZnO and In: ZnO for cost-effective photovoltaic device technology. *Micromachines*, *13*(11), 1966.

[69] El Hachimi, A. G., Zaari, H., Benyoussef, A., El Yadari, M., & El Kenz, A. (2014). First-principles prediction of the magnetism of 4f rare-earth-metal-doped wurtzite zinc oxide. *Journal of rare earths*, *32*(8), 715-721.

[70] Wu, Q., Liu, G., Shi, H., Zhang, B., Ning, J., Shao, T., ... & Zhang, F. (2023). Impact of Nd doping on electronic, optical, and magnetic properties of ZnO: A GGA+ U study. *Molecules*, *28*(21), 7416.

[71] Deng, S. H., Duan, M. Y., Xu, M., & He, L. (2011). Effect of La doping on the electronic structure and optical properties of ZnO. *Physica B: Condensed Matter*, *406*(11), 2314-2318.

[72] Meulenkamp, E. A. (1999). Electron transport in nanoparticulate ZnO films. *The Journal of Physical Chemistry B*, *103*(37), 7831-7838.

[73] Wang, B., Nagase, S., Zhao, J., & Wang, G. (2007). The stability and electronic structure of single-walled ZnO nanotubes by

density functional theory. *Nanotechnology*, *18*(34), 345706.

[74] Namisi, M. M., Musembi, R. J., Mulwa, W. M., & Aduda, B. O. (2023). DFT study of cubic, tetragonal and trigonal structures of KGeCl3 perovskites for photovoltaic applications. *Computational Condensed Matter*, *34*, e00772.

[75] Harun, K., Salleh, N. A., Deghfel, B., Yaakob, M. K., & Mohamad, A. A. (2020). DFT+ U calculations for electronic, structural, and optical properties of ZnO wurtzite structure: A review. *Results in Physics*, *16*, 102829.

[76] Berrezoug, H. I., Merad, A. E., Zerga, A., & Hassoun, Z. S. (2015). Simulation and modeling of structural stability, electronic structure and optical properties of ZnO. *Energy Procedia*, *74*, 1517-1524.

[77] Solola, G. T., Bamgbose, M. K., Adebambo, P. O., Ayedun, F., & Adebayo, G. A. (2023). First-principles investigations of structural, electronic, vibrational, and thermoelectric properties of half-Heusler VYGe (Y= Rh, Co, Ir) compounds. *Computational Condensed Matter*, e00827.